Dynamical analysis of low-energy electron-diffraction intensities from InAs(110)

C. B. Duke and A. Paton
Xerox Webster Research Center, Xerox Square W114, Rochester, New York 14644

A. Kahn and C. R. Bonapace
Department of Electrical Engineering and Computer Science, Princeton University, Princeton, New Jersey 08544

(Received 6 December 1982)

The measured intensities of 14 diffracted beams of low-energy ($30 \leq E \leq 240$ eV) electrons normally incident on InAs(110) are reported. The temperature of the InAs surface during the measurements was $T=110$ K. The surfaces were prepared by ion-bombardment and annealing cycles followed by a verification of surface stochiometry (to within 10%) via Auger electron spectroscopy. Two separate crystals were examined in two separate vacuum instruments in order to verify the reproducibility of the intensity data. The data were analyzed using a relativistic, Hara-exchange electron–ion-core potential and an x-ray R-factor structure-analysis methodology. This analysis leads to the best-fit structure of InAs(110) being a rotation of the uppermost layer with the As rotated outward and the In inward. The second layer also is reconstructed with the In being displaced upward by 0.07 ± 0.1 Å relative to its position in the bulk and the As being displaced downward by an equal amount. The x-ray R factor for the best-fit structure is $R_x=0.23$. This structure gives a satisfactory visual description of the measured intensities. For bond-length-conserving top-layer rotations the angle between the plane of the surface In-As chains and the plane of truncated bulk surface is $\omega_1=31° \pm 3°$, in accordance with expectations based on correlations of covalent radii with prior zinc-blende-structure compound-semiconductor surfaces. The structure of InAs(110) provides the first test of these correlations. The best-fit R-factor structure corresponds to reduced relaxation parallel to the surface of the top-layer As relative to that for the bond-length-conserving structure. This best-fit structure is, however, equivalent to its bond-length-conserving counterpart ($\omega_1=31°$) to within the accuracy of the R-factor methodology.

I. INTRODUCTION

During the past two decades the establishment of relationships between interface properties and the nature of interface chemical bonds has been a major and controversial topic in studies of semiconductor interfaces.[1–5] Although for molecules and bulk solids the traditional means for establishing such relationships is via comparisons of atomic geometries with various indices of the nature of the chemical bonds,[6–8] for interfaces the lack of structural information led to proposals of such relationships on the basis of comparisons of interface electrical properties with various measures of the strength of the bonds involved.[1–5] During the past five years, however, analyses of elastic low-energy electron diffraction (ELEED) intensities from the (110) (i.e., cleavage) surfaces of zinc-blende-structure compound semiconductors have begun to provide a comprehensive view[9] of the richness of surface structures evident on these homologous surfaces of materials whose bulk structures are identical[10] and whose bonding is nominally "covalent."[7,8] Most recently, an ELEED structure analysis[11] of GaSb(110) and its comparison with an extended structure analysis[12] for ZnTe(110) revealed that early suggestions[2,13–15] of correlations between surface structure and various measures[6,7] of bonding ionicity fail to describe the measured structures of the (110) surfaces of zinc-blende-structure semiconductors. In fact, this failure motivated the proposal[16] of new correlations of the (110) surface structures with the bulk lattice constants, the covalent radii, and the pseudopotential radii of the constituents of these materials. These proposed correlations were compatible with all (110) surface geometries known at the time and, of course, predicted certain features of the structures of the as-yet-unexamined surfaces.

Our purposes in this paper are to present and document our determination of the surface structure of

InAs(110) by ELEED intensity analysis and to show that the resulting structure substantiates the predictions of the proposed structure-atomic-size correlations. The definitions of the quantities specifying the atomic geometry of InAs(110) are given in Fig. 1 in which the bulk structural parameters reported in Wyckoff[10] are utilized for the dimensions of the surface unit cell. Our main result is that InAs may be characterized by a bond-length-conserving rotation of $\omega_1=31°\pm3°$ in the top layer in which the As moves outward and the In inward, as well as a counter distortion of the second layer in which the In moves upward and the As downward by 0.075 ± 0.05 Å. A slight improvement in the best-fit structure as determined by an R-factor minimization criterion can be achieved by permitting the top-layer As to relax parallel to the surface away from its rotated position about halfway back towards its undistorted position. The magnitude of this improvement lies, however, within the uncertainties inherent in the R-factor analysis methodology. The large value of the relative displacement of the In and As in the top layer normal to the surface, i.e., $\Delta_{1,\perp}=0.78$ Å, and the associated large value of $\omega_1=31°$ for a bond-length-conserving top-layer rotation, are precisely the surface structure features predicted from the structure-atomic-size correlations cited above.

We proceed by indicating the experimental procedures in Sec. II and defining our calculations in Sec. III. We present our structure analysis in Sec. IV and conclude with a discussion of our results.

II. EXPERIMENTAL PROCEDURES

Polished InAs(110) wafers (n-type) were obtained from Rockwell International. The samples were held by Mo foil on an ultrahigh-vacuum manipulator allowing ELEED data acquisition at or near liquid-nitrogen temperature. The experiments were performed, at pressures of 1.5×10^{-10} Torr, on two

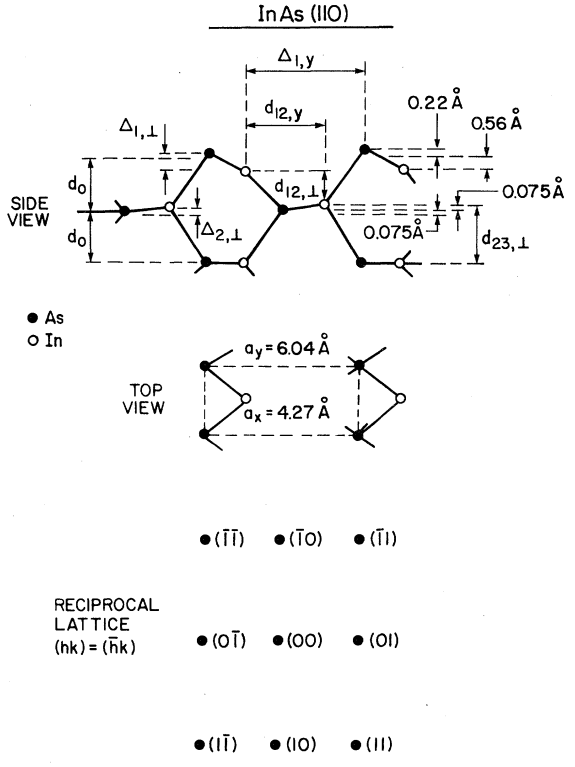

FIG. 1. Schematic indication of the surface atomic geometry and the associated ELEED normal incidence spot pattern for the (110) surface of InAs. The symbols utilized in Table I are defined in the upper panel of the figure. The numerical values shown are taken from panel (d) of Table I. The surface unit-cell parameters are those given by Wyckoff (Ref. 10).

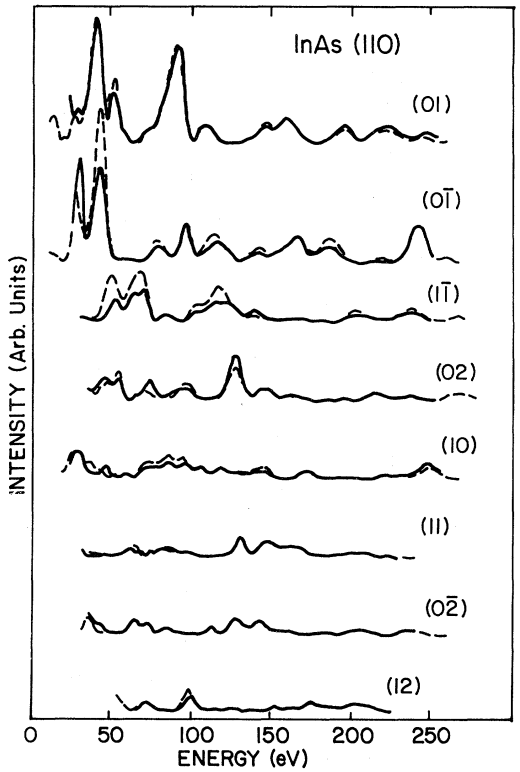

FIG. 2. Comparison of the measured intensity profiles for a particular crystal of InAs(110) (solid lines) with the average of three independent sets of these profiles for two crystals (dashed lines). All of the measurements were performed at $T\simeq110$ K.

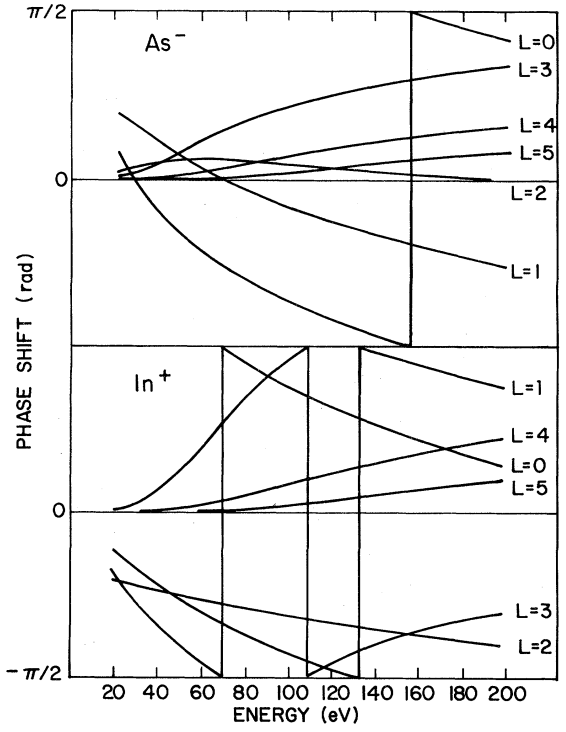

FIG. 3. Phase shifts for the In^+ and As^- species resulting from relativistic Hara exchange. Since the exchange depends on the energy of the incident electron, so do the muffin-tin radii and potentials, as described in the text.

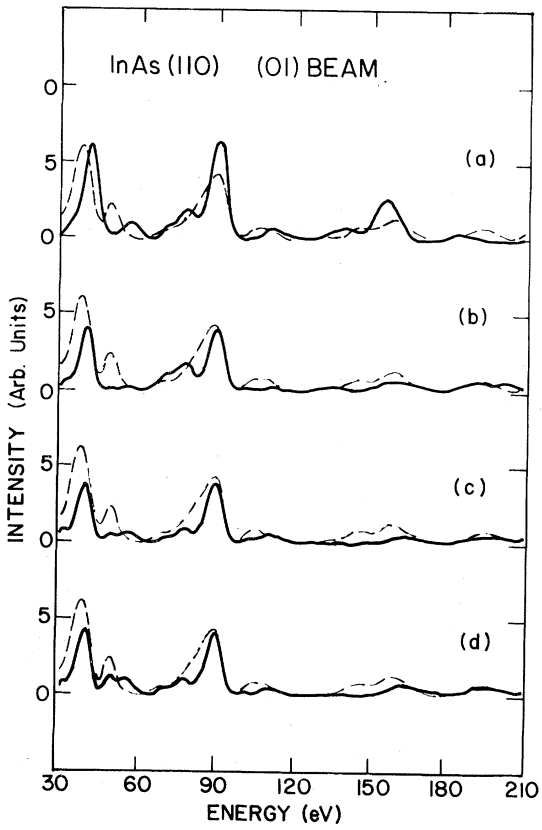

FIG. 4. Comparison of calculated (solid lines) and measured (dashed lines) intensities of electrons normally incident on InAs(110) diffracted into (01) beam. Panel (a): calculated intensities for the unreconstructed surface structure as specified in panel (a) of Table I. Panel (b): calculated intensities for the $\omega_1=31°$ bond-length-conserving top-layer rotation structure specified in panel (b) of Table I. Panel (c): calculated intensities for the same structure as panel (b) but with a second-layer shear of 0.15 Å as specified in panel (c) of Table I. Panel (d): calculated intensities for the same structure as panel (c) but with a reduced relaxation parallel to the surface of the As in the top layer as specified in panel (d) of Table I.

separate samples and in two different vacuum systems in order to ensure reproducibility of the data. The samples were prepared with a 1 keV-sputtering cycle in an ambient pressure of 3×10^{-5} Torr of research grade Ar followed by a 1-h annealing at 420 °C. The temperature was controlled with a Chromel-Alumel thermocouple welded on the Mo foil. Surface contamination and stoichiometry were monitored via Auger electron spectroscopy. Sharp, low-background (1×1) low-energy electron diffraction (LEED) patterns resulted from this procedure. The samples were cooled to 110 K to reduce the atomic vibrational amplitudes and thereby extend the useful range of the LEED intensity to above 240 eV. The Debye temperature of InAs is about 270 K at room temperature and 300 K at 110 K.[17]

The ELEED intensity profiles were recorded with a Gamma Scientific spot photometer and normalized to the beam current. The $(hk)=(\bar{h}k)$ symmetry, characteristic of all (110) zinc-blende surfaces, was carefully monitored. Three sets of data were recorded. Each set included 14 beams, i.e., those with the beam indices (01), (10)=($\bar{1}$0), (11)=($\bar{1}$1), (1$\bar{1}$)=($\bar{1}\bar{1}$), (0$\bar{1}$), (02), (12)=($\bar{1}$2), (21)=($\bar{2}$1), (0$\bar{2}$), ($\bar{1}$2)=(1$\bar{2}$), (2$\bar{1}$)=($\bar{2}$1), (20)=($\bar{2}$0), (13)=($\bar{1}$3), and (1$\bar{3}$)=($\bar{1}\bar{3}$). In Fig. 2 we illustrate the reproducibility of the measured ELEED intensities by comparing one set with the average of the three sets. Five of these beams, the (01), (0$\bar{1}$), (1$\bar{1}$), (02), and (10) are much more intense than the rest. The (11) and (0$\bar{2}$) beams are of medium intensity, whereas the (12), ($\bar{1}$2), (13), (20), ($\bar{2}$1), (21), and($\bar{1}$3) beams are weak.

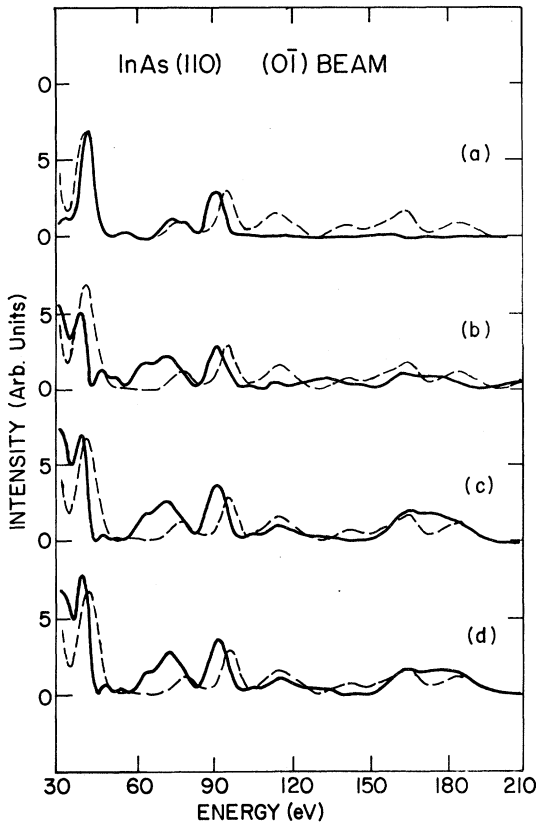

FIG. 5. Same as Fig. 4 for the (0$\bar{1}$) beam.

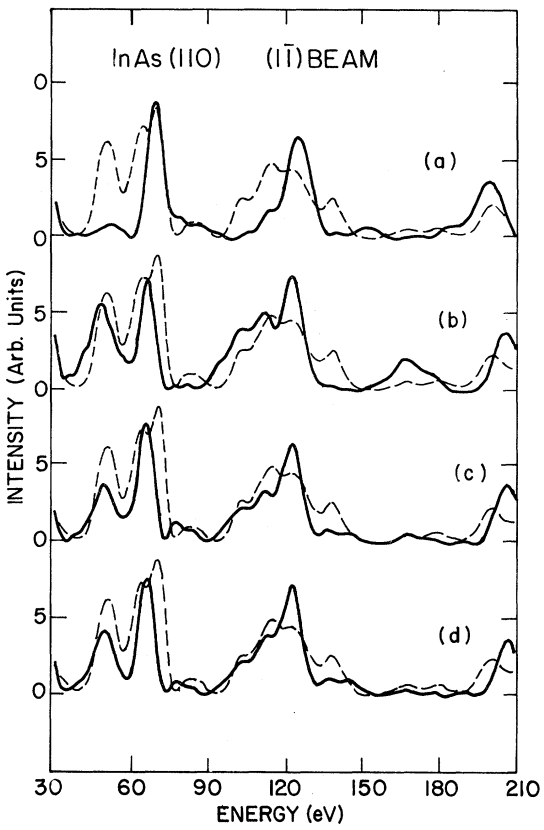

FIG. 6. Same as Fig. 3 for the (1$\bar{1}$) beam.

III. MODEL CALCULATIONS

An approximate multiple-scattering model of the diffraction process, described previously,[18] was used to perform our dynamical calculations of the ELEED intensities. In this model the scattering species are represented by energy-dependent phase shifts in terms of which the ELEED intensities from the surface are computed. Each atomic bilayer (see Fig. 1) parallel to the surface is divided into two sublattices, each of which consists of all In or all As species, respectively.[19] The scattering amplitudes for each sublattice are evaluated analytically whereas the scattering between sublattices is described by a set of coupled matrix equations expressed in the angular momentum respresentation.[19,20] These equations are solved exactly for the uppermost three bilayers. For deeper (unreconstructed) bilayers the scattering amplitudes for each bilayer are obtained by considering the multiple scattering between the two subplanes within the bilayer but neglecting the multiple scattering between that bilayer and its neighbors. The calculated ELEED intensities are expressed in terms of a superposition of the scattering amplitudes for the individual bilayers. The formulas resulting from this prescription, the construction of the computer program embodying them, and the convergence tests of this program have been described in detail elsewhere.[18,21] The convergence tests revealed that the consideration of a slab of six atomic layers and the use of six phase shifts for each scatterer yield predicted intensities which are generally accurate to within a few percent, so these parameters were adopted for the calculations presented herein.

The electron—ion-core interaction is described by a one-electron muffin-tin potential. The one-electron crystal potential is formed from a superposition of overlapping ionic (e.g., In^+ and As^-) relativistic charge densities. These charge densities are obtained via self-consistent solutions to the Dirac equation for the individual ionic species. Given the charge densities, the phase shifts are evaluated by solving the nonrelativistic Schrödinger equation using the (energy-dependent) Hara model for the exchange potential.[22,23] A muffin-tin approximation to the crystal potential is imposed prior to the calculation of the phase shifts. The muffin-tin radii are taken to be the values at which the potentials of the

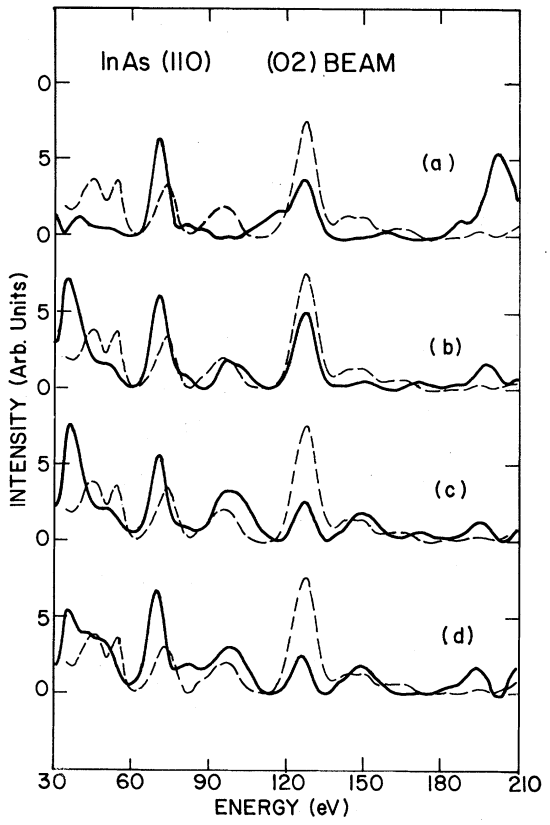

FIG. 7. Same as Fig. 4 for the (02) beam.

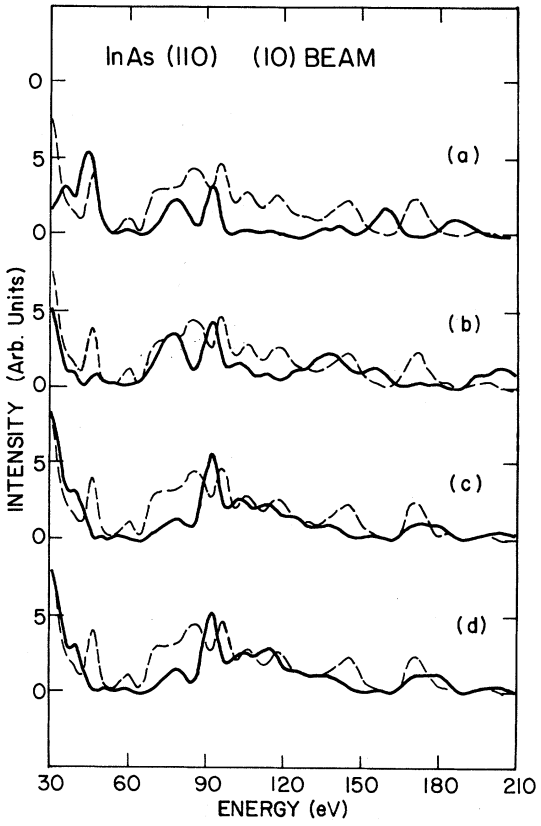

FIG. 8. Same as Fig. 4 for the (10) beam.

In^+ and As^- cross, and the potential outside the muffin-tin spheres is taken to be the calculated value at the crossover point. Because the exchange potential depends on the energy of the incident electron, the crossover point and, hence, the muffin-tin (MT) radii and crossover potentials also depend on this energy. Values of the radii are essentially constant at $r_{MT}(In^+)=1.26$ Å and $r_{MT}(As^-)=1.36$ Å over the range of beam energies 30 eV $\leq E \leq$ 240 eV. The muffin-tin potential decreases from 10.6 eV at $E=30$ eV to 10.0 eV at $E=240$ eV. The phase shifts associated with these potentials are shown in Fig. 3. We have shown earlier for both ZnO (Ref. 24) and GaAs (Ref. 25) that the phase shifts resulting from this procedure are essentially identical to those obtained when neutral (i.e., In and As) atomic potentials are utilized.

The electron-electron interaction is incorporated into the model via complex inner potential with a constant real part V_0 and an imaginary part characterized by the inelastic collision mean free path λ_{ee}.[19] We selected V_0 to minimize the x-ray R factor[26] [given by Eqs. (3), (8), (13), (14), and (16) of Ref. 26]. Our major structure searches were performed using $\lambda_{ee}=12$ Å, although we examined the sensitivity of the values of the R factors to the value of λ_{ee}.

The consequences of thermal lattice vibrations are neglected in the structure search reported herein, because previous studies of GaAs(110) (Ref. 18) and GaP(110) (Ref. 27) revealed that incorporation of bulk lattice vibrations into the model not affect the results of the structure analysis. These consequences are not expected to be important in the analysis of ELEED intensity data taken with a spot photometer at temperatures well below the Debye temperature,[18,19] which in the case of InAs is approximately 300 K.[17]

IV. STRUCTURE ANALYSIS

Our analysis of the ELEED intensity data to extract the surface atomic geometry of InAs(110) proceeded in a fashion analogous to that utilized previously for GaSb(110) (Ref. 11) and ZnTe(110) (Ref. 12). ELEED intensities were calculated for the unreconstructed geometry. This structure is specified in row (a) of Table I. The resulting ELEED intensities are compared with the measured ones for the nine strongest beams in panels (a) of Figs. 4—12.

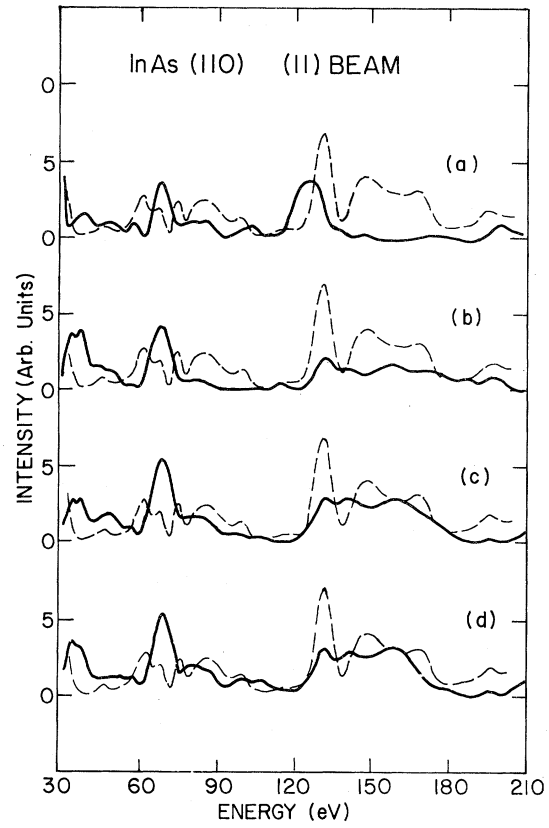

FIG. 9. Same as Fig. 4 for the (11) beam.

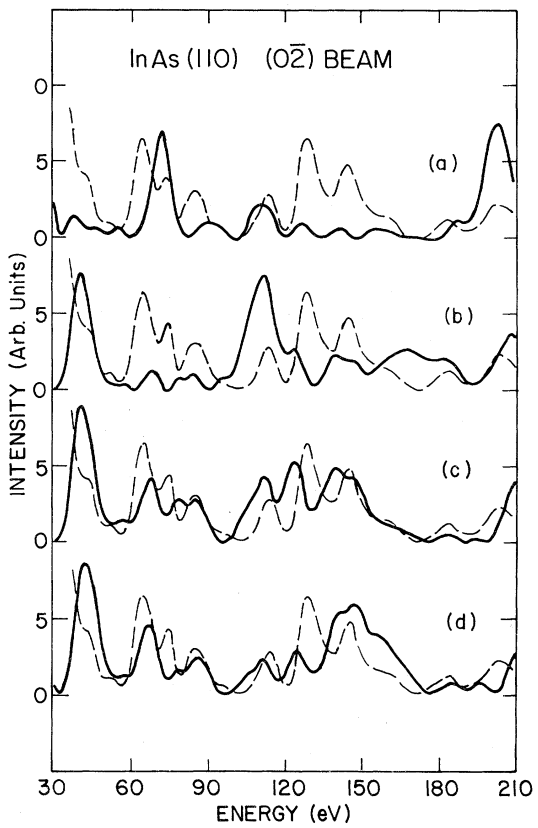

FIG. 10. Same as Fig. 4 for the (0$\bar{2}$) beam.

These figures are presented in order of the decreasing intensities of the beams [e.g., the (01) is stronger than the (0$\bar{1}$), etc.]. It is evident from the figures that the unreconstructed geometry provides a poor description of many beams and hence may be eliminated as an acceptable structure for InAs(110). We must, therefore, undertake a systematic search of possible reconstructed surface geometries. We perform this search in two steps. First, we indicate the independent structural variables which describe a reconstructed InAs(110) surface geometry. Second, we determine the "optimum" values of these variables by minimization of the x-ray R factor.[11,12,27]

The structural variables which characterize the atomic geometries of the (110) surfaces of zinc-blende-structure compound semiconductors are specified in Fig. 1. The vector shear between the In and As in each layer, $\vec{\Delta}_i$, has two independent components: one normal to the surface, $\Delta_{i,\perp}$, and one along the y axis, $\Delta_{i,y}$. The symmetry of the measured intensities requires that $\Delta_{i,x}$ equal its value in the bulk.[18] It has become customary to perform structure searches by initially linking the values of $\Delta_{1,\perp}$ and $\Delta_{1,y}$ in such a fashion that all the bond lengths remain constant as the surface species are displaced from their bulk positions ("bond-length-conserving" rotations). In this case, the angle ω_1 between the plane of the uppermost chain of In and As and that of the truncated bulk surface is utilized as the independent structural variable (see, e.g., Table I). We follow that procedure here, utilizing variations in ω_1 for bond-length-conserving rotations to fix $\Delta_{1,\perp}$ and subsequently varying $\Delta_{1,y}$ independently in order to determine the shear vector $\vec{\Delta}_1$, characteristic of the uppermost layer of In and As species. The third independent structural variable is taken to be the uppermost layer spacing, $d_{12,\perp}$. Finally, we define the shear vector in the second layer $\vec{\Delta}_2$ by its perpendicular component $\Delta_{2,\perp}$ alone because the ELEED analysis is not sufficiently accurate to determine ω_2 or $\Delta_{2,y}$ separately, although we expect bond-length-conserving structures for the second layer.[28] Therefore, $\Delta_{1,\perp}$, $\Delta_{1,y}$, $d_{12,\perp}$, and $\Delta_{2,\perp}$ are the four independent quantities in terms of which the two-layer reconstructions of the (110) surfaces of InAs are specified.

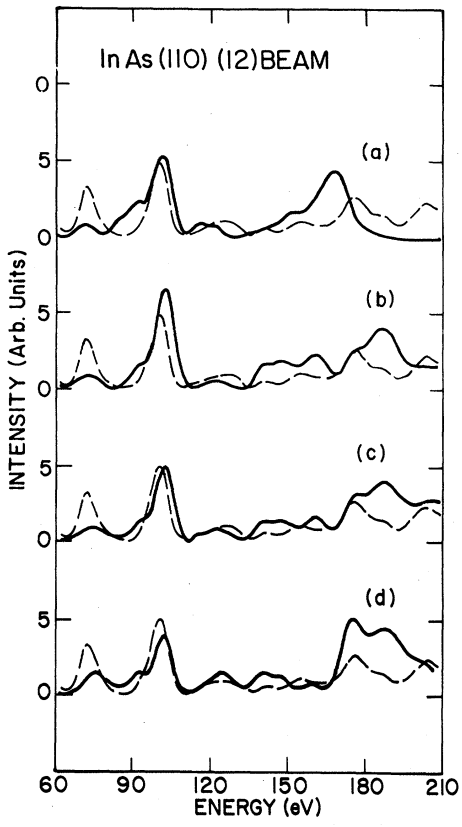

FIG. 11. Same as Fig. 4 for the (12) beam.

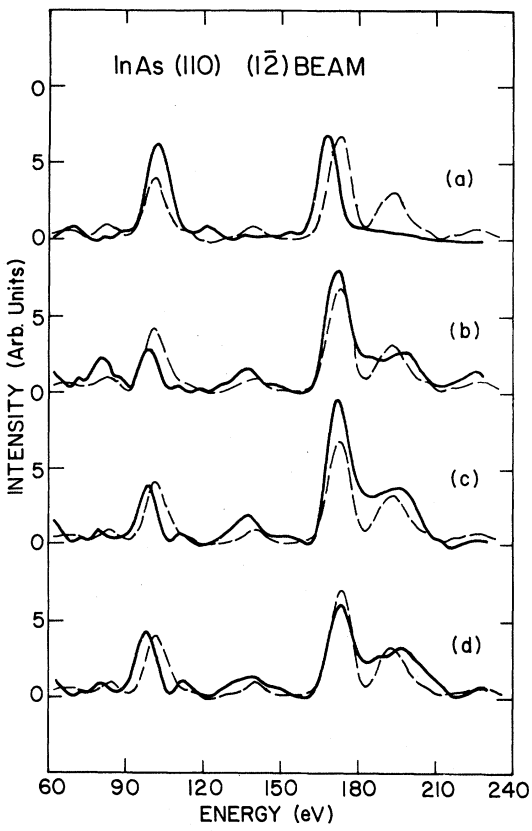

FIG. 12. Same as Fig. 4 for the (1$\bar{2}$) beam.

Having defined the independent structural variables, we proceed with a description of the R-factor structure analysis. First, we calculate the ELEED intensities and from them the x-ray structure factors for a range of bond-length-conserving top-layer reconstructions described by $0 \leq \omega_1 \leq 34.8°$. The resulting values of R_x are shown in the top panel of Fig. 13. We find that two minima occur: one near $\omega_1 = 0$ and the other for $\omega_1 = 31°$. The minimum near $\omega_1 = 0$ is not used as a starting point for refining the structure because the relative intensities of the various diffracted beams are inadequately described by structures in that vicinity of values of $\Delta_{1,\perp}$.[29] The bond-length-conserving top-layer rotation characterized by $\omega_1 = 31°$ is specified in panel (b) of Table I. Comparisons of the intensities calculated using this surface geometry with the measured ELEED intensities are given in panels (b) of Figs. 4–12.

We initially refine the $\omega_1 = 31°$ bond-length-conserving top-layer rotation structure by varying the spacing between the uppermost layer and substrate, i.e., $d_{12,\perp}$. The resulting values of R_x are shown in panel (b) of Fig. 13. Relaxations of ± 0.1 Å increased R_x by 0.07, well outside the $\Delta R(\text{threshold}) = 0.04$ bound for absolute discrimination against a structure.[27] Thus we conclude from Fig. 13 that the spacing between the uppermost two layers is equal to its value for the bond-length-conserving top-layer rotation to within ± 0.05 Å.

Another refinement of the $\omega_1 = 31°$ bond-length-conserving rotation is achieved via an examination of variations in the second-layer In-As displacement normal to the surface (i.e., $\Delta_{2,\perp}$). The associated variations in R_x are shown in panel (c) of Fig. 13. The minimum-R_x structure resulting from this refinement is specified in panel (c) of Table I. Comparisons of the associated calculated intensities with the measured ones are given in panels (c) of Figs. 4–12. Evidently, a small ($\Delta_{2,\perp} = -0.15$ Å) shear is suggested, but is not required because it yields $\Delta R_x = 0.03$ relative to the bond-length-conserving top-layer rotation alone: a value of ΔR_x which is less than the $\Delta R(\text{threshold}) = 0.04$ required for absolute discrimination in favor of a structure.

Finally, we refined the optimum R_x structure specified in panel (c) of Table I by varying the magnitude of the In-As shear in the top layer parallel to the surface, i.e., the value of $\Delta_{1,y}$. The consequences of this examination are presented in panel (d) of Fig.

TABLE I. Candidate structures for the surface atomic geometry of InAs(110). The structural symbols Δ and d are defined in Fig. 1. The angle between the actual plane of the uppermost chain of In and As and the plane of the truncated bulk surface is designated by ω_1. The inner potential symbol V_0, as well as the R factors R_x, are defined in the text. $\lambda_{ee}=12$ Å for all the calculated R factors in the table.

Structure	Layer	As	In	$\Delta_{1,\perp}$ (Å)	$\Delta_{2,\perp}$ (Å)	$d_{12,\perp}$ (Å)	$d_{23,\perp}$ (Å)	Δ_{1y} (Å)	$d_{12,y}$ (Å)	ω_1 (deg)	In_1-As_1 % Bond-length change	In_1-As_2 % Bond-length change	As_1-In_2 % Bond-length change	V_0 (eV)	λ_{ee} (Å)	R_x
(a)																
Unreconstructed	1	0	0	0	0	2.134	2.134	4.527	3.018	0	0	0	0	12	12	0.38
(b)																
Best bond-length-conserving top-layer rotation	1	↑0.22	↓0.56	0.78	0	1.572	2.134	4.743	3.597	31.0	0	0	0	12	12	0.28
(c)																
Best top-layer rotation and second-layer shear	1	↑0.22	↓0.56	0.78	−0.15	1.497	2.209	4.743	3.597	31.0	0	1.75	−2.57	12	12	0.25
	2	↓0.075	↑0.075													
(d)																
Best fit	1	↑0.22	↓0.56	0.78	−0.15	1.497	2.209	4.985	3.597	36.5	−4.25	1.75	1.93	12	12	0.23
	2	↓0.075	↑0.075													

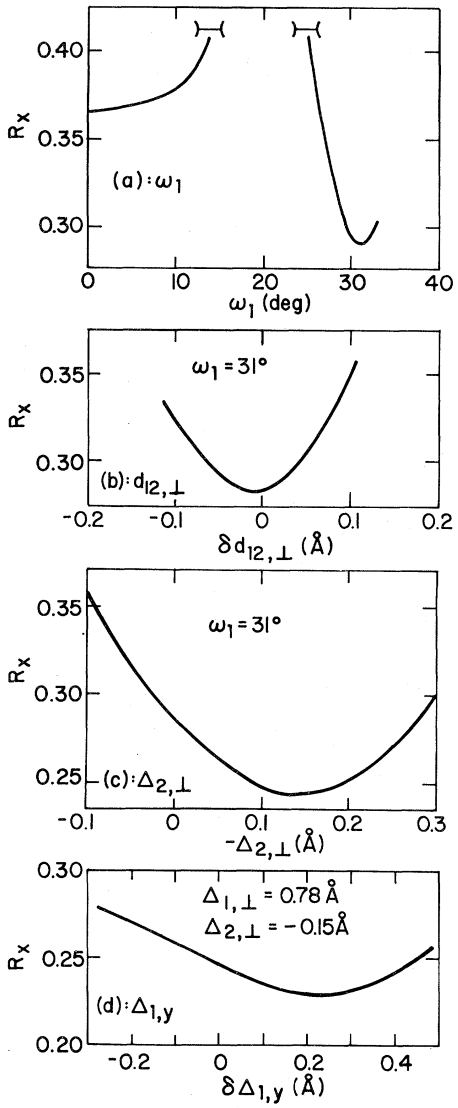

FIG. 13. Values of the x-ray R factors associated with systematic variations of the parameters characteristic of the surface reconstruction of InAs(110). Panel (a): variations of ω_1 for a bond-length-conserving top-layer rotation. Panel (b): variations of the spacing between the top layer and the layer beneath relative to its value for an $\omega_1=31°$ bond-length-conserving top-layer rotation alone. Panel (c): variations in the second-layer shear relative to its initial value of zero for an $\omega_1=31°$ top-layer rotation. Panel (d): variations in the position of the top-layer As parallel to the y axis relative to its value for an $\omega_1=31°$ bond-length-conserving top-layer rotation. A shear of $\Delta_{2,\perp}=-0.15$ Å in the second layer was utilized in evaluating this panel.

13. It is noteworthy that the best-fit structure occurs for a value of $\Delta_{1,y}$ which differs from that characteristic of a bond-length-conserving rotation. Hence, the value of ω_1 varies accordingly as evident

from panel (d) of Table I in which the overall minimum-R_x structure is specified. Further, small refinements about the minimum-R_x structure were attempted in order to recover any additional effects of interactions among the structural variables in their four-parameter $(\Delta_{1,\perp},\Delta_{1,y},d_{12,\perp},\Delta_{2,\perp})$ space. None were observed, so panel (d) of Table I contains the optimal structure obtained by minimizing R_x. Comparisons of the measured intensities with those calculated for this structure are given in panels (d) of Figs. 4–12.

The accuracy with which the minimum-R_x analysis specifies the four structural parameters $\Delta_{1,\perp},d_{12,\perp},\Delta_{2,\perp}$, and $\Delta_{1,y}$ may be ascertained from Fig. 13. An earlier analysis[27] of the precision of the procedure revealed that for a fixed model of the electron-solid interaction, a change in R_x of $\Delta R_x=0.04$ was sufficient to ensure discrimination against a structure. Using this criterion we obtain $\Delta_{1,\perp}=0.78\pm0.05$ Å, $d_{12,\perp}=1.50\pm0.08$ Å, $\Delta_{2,\perp}=-0.15\pm0.2$ Å, and $\Delta_{1,y}=4.99\pm0.4$ Å, as the *maximal* uncertainties in the best-fit structure given in panel (d) of Table I. The uncertainties in $\Delta_{1,\perp}$ are related to those in ω_1 for bond-length-conserving top-layer rotations by noting that for these rotations

$$\omega_1=\sin^{-1}(4\Delta_{1,\perp}/a_y) \ . \tag{1}$$

Thus the uncertainties in ω_1 for such rotations [obtained, e.g., from panel (a) of Fig. 13], i.e., $28°\leq\omega_1\leq34°$, are a direct consequence of the high accuracy (±0.05 Å) with which $\Delta_{1,\perp}$ is determined by ELEED intensity analysis.[28] Since $\Delta_{1,y}$ is determined less accurately, however, the uncertainties in ω_1 are far larger for reconstructions which do *not* conserve bond lengths than the values obtained from panel (a) of Fig. 13. This result is manifested in Table I by the fact that the value of $\omega_1=36.5°$ for the best-fit (i.e., relaxed $\Delta_{1,y}$) structure lies well outside the range $28°\leq\omega_1\leq34°$ determined from panel (a) of Fig. 13 for bond-length-conserving top-layer rotations. The best-fit structure [panel (d), Table I] yields a value of R_x which differs from its bond-length-conserving top-layer analog [panel (c), Table I] only by $\Delta R_x=0.02$, however, well inside $\Delta R(\text{threshold})=0.04$. Therefore within the uncertainties inherent in the analysis, the minimum-R_x structure is equivalent to the bond-length-conserving top-layer rotation structure specified in panel (c) of Table I.

V. SUMMARY AND DISCUSSION

The ELEED intensity analysis reported in Sec. IV reveals that InAs(110) exhibits a reconstruction at $T=110$ K. A bond-length-conserving top-layer rotation of the As upward and In downward by $\omega_1=31°\pm3°$ is compatible with the ELEED intensity data, although an As relaxation parallel to the surface of less than that associated with the bond-rotated structure is slightly preferred by the minimum R-factor criterion. The second layer exhibits a counter rotation of the In upward and As downward, characterized by an In-As shear normal to the surface of $\Delta_{2,\perp}=-0.15\pm0.2$ Å. The final ranges of the four independent structural variables defined in Sec. IV are $0.73\text{ Å}\leq\Delta_{1,\perp}\leq0.83$ Å, $4.6\text{ Å}\leq\Delta_{1,y}\leq5.4$ Å, $-0.35\text{ Å}\leq\Delta_{2,\perp}\leq0.05$ Å, and $1.42\text{ Å}\leq d_{12,\perp}\leq1.58$ Å. The main significance of this structure is its confirmation of the prediction[16] that the value of $\Delta_{1,\perp}$ should be $\Delta_{1,\perp}=0.73$ Å (to within an accuracy of ±0.05 Å) based on the value of the lattice constant of InAs ($a_0=6.036$ Å at room temperature[10]) or the sum of its pseudopotential radii.[30] For bond-length-conserving top-layer reconstructions, independent correlations of ω_1 with lattice constants or pseudopotential radii predicted[16] that ω_1 should be $\omega_1=29°$ to within $\pm3°$. This prediction also is in accord with the measured range of $\omega_1=31°\pm3°$ [obtained from panel (c) of Table I and panel (a) of Fig. 13] for this class of reconstruction. Therefore InAs(110) is the first test case to confirm the concept that atomic sizes rather than bonding ionicities determine the atomic geometries of compound semiconductor surfaces.

ACKNOWLEDGMENTS

The authors are indebted to Dr. W. J. Shaffer of Rockwell International for providing the InAs samples, to L. J. Kennedy for assistance, and to Dr. M. D. Tabak for his generous support of this work.

[1]C. A. Mead, Solid State Electron. 9, 1023 (1966).
[2]J. C. Phillips, Solid State Commun. 12, 861 (1973).
[3]C. B. Duke, Mater, Sci. Eng. 25, 13 (1976).
[4]W. E. Spicer, I. Landau, P. Skeath, and C. Y. Su, J. Vac. Sci. Technol. 17, 1019 (1980).
[5]L. J. Brillson, J. Vac. Sci. Technol. 20, 652 (1982).
[6]L. Pauling, *The Nature of the Chemical Bond,* 3rd ed. (Cornell University Press, Ithaca, 1973), p. 93.
[7]J. C. Phillips, Rev. Mod. Phys. 42, 317 (1970).
[8]*Structure and Bonding in Crystals,* edited by M. O'Keeffe and A. Navrotsky (Academic, New York, 1981), Vol. 1.
[9]C. B. Duke, Adv. Ceram. 4, 1 (1983).

[10]R. W. G. Wyckoff, *Crystal Structures* (Wiley, New York, 1963), Vol. I, p. 108.
[11]C. B. Duke, A. Paton, and A. Kahn, Phys. Rev. B 27, 3436 (1983).
[12]C. B. Duke, A. Paton, and A. Kahn, J. Vac. Sci. Technol. A (in press).
[13]S. Kurtin, T. C. McGill, and C. A. Mead, Phys. Rev. Lett. 22, 1433 (1969).
[14]C. B. Duke, A. R. Lubinsky, B. W. Lee, and P. Mark, J. Vac. Sci. Technol. 13, 761 (1976).
[15]C. B. Duke, R. J. Meyer, and P. Mark, J. Vac. Sci. Technol. 17, 971 (1980).
[16]C. B. Duke, J. Vac. Sci. Technol. B (in press).
[17]O. Madelung, *Physics of III-V Compounds* (Wiley, New York, 1964).
[18]R. J. Meyer, C. B. Duke, A. Paton, A. Kahn, E. So, J. L. Yeh, and P. Mark, Phys. Rev. B 19, 5194 (1979).
[19]C. B. Duke, Adv. Chem. Phys. 27, 1 (1974); in *Dynamic Aspects of Surface Physics, Proceedings of the International School of Physics "Enrico Fermi," Course LVIII,* edited by F. O. Goodman (Editrice Compositori, Bologna, 1974), pp. 99—173.
[20]G. E. Laramore and C. B. Duke, Phys. Rev. B 5, 267 (1972).
[21]R. J. Meyer, C. B. Duke, A. Paton, E. So, J. L. Yeh, A. Kahn, and P. Mark, Phys. Rev. B 22, 2875 (1980).
[22]S. Hara, J. Phys. Soc. Jpn. 22, 710 (1967).
[23]W. K. Ford, C. B. Duke, and A. Paton, Surf. Sci 115, 195 (1982).
[24]C. B. Duke and A. R. Lubinsky, Surf. Sci. 50, 605 (1975).
[25]C. B. Duke, A. Paton, W. K. Ford, A. Kahn, and J. Carelli, Phys. Rev. B 26, 803 (1982).
[26]E. Zanazzi and F. Jona, Surf. Sci. 62, 61 (1977).
[27]C. B. Duke, A. Paton, W. K. Ford, A. Kahn, and J. Carelli, Phys. Rev. B 24, 562 (1981).
[28]C. B. Duke, R. J. Meyer, A. Paton, P. Mark, A. Kahn, E. So, and J. L. Yeh, J. Vac. Sci. Technol. 16, 1252 (1979).
[29]C. B. Duke, S. L. Richardson, A. Paton, and A. Kahn, Surf. Sci. Lett. (in press).
[30]A. Zunger and M. L. Cohen, Phys. Rev. B 20, 4082 (1979).